Available online at www.sciencedirect.com
ScienceDirect
International Journal of Heat and Mass Transfer 51 (2008) 3298–3308
International Journal of HEAT and MASS TRANSFER
www.elsevier.com/locate/ijhmt

Heat transfer study in a discoidal system: The influence of rotation and space between disks

Julien Pellé *, Souad Harmand

Laboratoire de Mécanique et Energétique, Université de Valenciennes et du Hainaut-Cambrésis, Le Mont Houy, 59313 Valenciennes Cedex 9, France

Received 6 April 2007; received in revised form 21 October 2007
Available online 29 January 2008

Abstract

This article presents an experimental study of the local heat transfer on the rotor surface in a discoidal rotor–stator system air-gap in which an air jet comes through the stator and impinges the rotor. To determine the surface temperatures, measurements were taken on the rotor, using an experimental technique based on infrared thermography. A thermal balance was used to identify the local convective heat transfer coefficient. The influence of the dimensionless spacing interval G between the disks and of the rotational Reynolds number Re was measured and compared with the data available in bibliography. Local convective heat transfer coefficients were obtained for an axial Reynolds number $Re_j = 41.6 \times 10^3$, a rotational Reynolds number Re between 0.2×10^5 and 5.16×10^5, and a dimensionless spacing interval G ranging from 0.01 to 0.16.

Keywords: Rotor–stator; Infrared thermography; Convective heat transfer; Impinging jet

1. Introduction

Nowadays, the power production industry is confronted with new challenges due to the need for sustainable development. For example, studies about wind generators have become more and more numerous. In fact, industry has worked to increase power production by attempting to increase generator efficiency. Industrialists (e.g., the Areva Group) have gotten involved in the development of discoidal rotor–stator systems. These systems do not use gears in order to avoid altering the system's mechanical efficiency, and are thus able to produce a lot of power at low rotational speeds. However, the increased production leads to inefficient cooling, generally due to the effect of rotation, making it imperative to improve cooling techniques in order to preserve the stability and reliability of many rotating systems. Knowledge of the parameters that influence the convective heat transfer in the air-gap can help manufacturers to better design their discoidal generators in order to avoid overheating. This particular industrial problem serves to underscore the importance of the more general problem of convective heat transfer and the flow structure in the air-gap of a discoidal system. In our study of this general problem, an impinging jet, passing through the center of the stator and coming into direct contact with rotor, was added in order to improve the motor's cooling method.

2. Bibliography review

2.1. Generalities about rotating disks

Von Karman [1] was the first author to describe the air flow around a rotating disk and to identify the boundary layer that develops near such a disk. There are two significant velocity components inside that boundary layer: the first one is radial, highlighting the effect of inertia due to the rotation, and the second is tangential, highlighting the effect of air viscosity. The convective heat transfer on a rotating disk have also been studied by Goldstein [2],

* Corresponding author. Fax: +33 327 511 961.
E-mail address: jpelle@univ-valenciennes.fr (J. Pellé).

0017-9310/$ - see front matter © 2007 Elsevier Ltd. All rights reserved.
doi:10.1016/j.ijheatmasstransfer.2007.11.037

Nomenclature

D	pipe diameter, m
e	spacing between the two disks, m
F	view factor
J_r	rotor radiosity, W m^{-2}
r	radius, m
R	outer radius of rotor, m
h	convective heat transfer coefficient, W m^{-2} K^{-1}
$\overline{h}$	mean convective heat transfer coefficient, W m^{-2} K^{-1}
q_v	flow rate, m^3 s^{-1}
T	temperature, K
$T(r,x)$	temperature inside zircon, K
T_∞	atmospheric temperature, K
V	velocity, m s^{-1}
x	axial position, m

Greek symbols

ΔH	height read on manometer, mm
ϵ	emissivity
τ	air transmission coefficient
ν	kinematic viscosity, m^2 s^{-1}
ω	rotational velocity, rad s^{-1}
λ	thermal conductivity, W m^{-1} K^{-1}
κ	flow parameter
ϕ	heat flux, W
φ	heat flux density, W m^{-2}
ρ	density, kg m^{-3}

Subscripts and superscripts

air	air
cv	convection
cd	conduction
env	environment
H_2O	water
j	jet
lam	laminar flow
mmH_2O	millimeter of water
pitot	Pitot tube
rad	radiation
stator	stator
θ	tangential
tur	turbulent flow
zir	zircone

Dimensionless numbers

C_W	flow rate coefficient $= q_v/\nu_{air}r$
G	dimensionless spacing $= e/R$
$\tilde{r}$	dimensionless radius $= r/R$
Re_r	local Reynolds number $= \omega r^2/\nu_{air}$
Re	rotational Reynolds number $= \omega R^2/\nu_{air}$
Re_j	jet Reynolds number $= V_j D/\nu_{air}$
Nu_r	local Nusselt number $= hr/\lambda_{air}$
$\overline{Nu}$	global Nusselt number $= \overline{h}R/\lambda_{air}$

Cobb and Saunders [3] and Richardson and Saunders [4] and Dorfman [5]. Dorfman [5] has suggested many correlations for both local and global Nusselt numbers, taking the radial temperature profile of the disk surface into account. More recently, Cardone [6] has proposed a correlation for when the flow is in transition between the laminar and the turbulent flow.

To improve surface cooling, several authors have studied the influence of jet impingement, for example, Huang [7], or Fenot [8]. Angioletti et al. [9] have concluded that heat transfer increases when the boundary layer near the surface is perturbed and the air is renewed. Other authors have studied mass and heat transfer changes in a single rotating disk configuration. Chen et al. [10] and Owen and Rogers [11] have examined the sensitivity of Nusselt numbers to jet diameter D, to the jet's Reynolds number Re_j, and to the distance between the jet outlet and the disk e/D.

Popiel and Boguslawski [12] have distinguished three flow zones on a rotating disk. The first one is the area of the disk where the jet's influence on the heat transfer is greatest. The second one is the area where rotation has the greatest effect. The third is a mixture of the first two. Chen et al. [10] concluded that the location of these zones depends on the ratio of the jet and rotation mass flow rates. They also note that the heat transfer on a rotating disk is modified by the jet when $Re_r < 200{,}000$. For greater values, the jet does not affect the local heat transfer. Axcell [13] has studied the influence of rugosity in a rotating disk configuration subjected to jet impingement. His use of a modified Reynolds number Re_m to take the effects of the jet and the rotation into account, such that $Re_m = \sqrt{Re_r^2 + Re_j^2\left(\frac{r}{D}\right)^2}$, seems to be appropriate.

Iacovides and Chew [14] have numerically studied three configurations of rotating cavity: with flow entering axially at the center and leaving radially through the outer shroud, with central axial throughflow, and a rotor–stator system with axial flow injection through the stator center and outflow through the annulus formed between the rotor disc and the outer shroud. More recently, Djaoui et al. [15] used a theoritcal and experimental approaches to produce a better understanding of the flow and heat transfer process occuring in a rotor–stator system subjected to a superposed radial inflow. They have studied the local Nusselt number on the stator. They mainly noticed a sudden decrease in the local Nusselt number when reaching the air-gap outet, which was explained by peripheral effects. They conclude that the main effect of the radial superimposed inflow is

to enhance the level of the core swirl ratio near the axis and, at the same time, to increase the heat transfer coefficient on the stator. Also, in 2007, Poncet and Shiestel [16] have numerically studied three configurations of rotor–stator cavities with throughflow. None of these studied cases focused on the convective heat transfer on the rotor. One of them allowed the author to compare their results to [15]. They also try to compare their results to those obtained by Sparrow and Goldstein [17].

Absent from this general information is any reference to a study of the influence of jet impingement on the heat transfers on the rotor of a discoidal rotor–stator system. We decided to examine the effect of an air jet on the cooling of a rotating disk in a discoidal rotor–stator system. We chose to position the jet in our experiment so that it would impinge at the center of the rotor, because it is the position which allows the best cooling [10]. Owen and Rogers [11] have studied the air flows in such a configuration and the next section provides a brief description of their research.

2.2. Rotor–stator configuration with an axial flow

Owen and Rogers [11] identify four possible flow configurations, depending on the Reynolds number and on the dimensionless spacing interval G.

2.2.1. Configuration I

In the case of a narrow dimensionless spacing interval and a laminar flow, the flow structure depends on the diameter of the opening and the injected mass flow rate. Soo [18] has solved Navier–Stokes equations theoretically and showed that the flow structure depends on a parameter, such as

$$\Phi(\tilde{r}) = \frac{GC_W}{2\pi \times (Re_G \tilde{r})^2} \tag{1}$$

If there is no opening in the center of the stator, this parameter is null, and the flow is centrifugal near the rotor and centripetal near the stator. The boundary layers are merged, and the flow is a Couette-type flow. For Soo [18], when $\Phi(\tilde{r}) < 0.01$, the flow conforms to the above description. In the other cases, the flow is centrifugal across the entire width of the air-gap. When a flow enters the air-gap via the opening in the stator, the appearance radius of the centripetal flow increases. In fact, given a significant injected mass flow rate, this centripetal flow can be totally absent from the air-gap.

2.2.2. Configuration III

For a narrow spacing interval between the two disks and a turbulent flow, the flow structure is identical to the laminar case. When the injected flow rate is very high and the rotational velocity of the rotor relatively low, the flow parameter $\lambda_0 = C_W Re^{-0.75}$ tends toward infinity. Consequently, the local and mean heat transfers tend toward a limit, which is determined using the moment coefficient and shear stresses, such that:

$$\tau_\theta = -0.0288[GRe(\tilde{r}(1-\beta))^{-7}]^{-0.25} F \rho_{air} \omega^2 R^2 \tag{2}$$

$$C_M = 0.0707(GRe)^{-0.25} \tag{3}$$

where $\beta = \frac{V_{\theta,\text{median}}}{\omega r}$.

However, for a high Reynolds number and a low injected flow rate ($\lambda_0 \to 0$), the following result is obtained:

$$C_M = 0.021(GRe)^{-0.25} \tag{4}$$

2.2.3. Configuration II

In this configuration, the spacing interval G is wide and the flow is laminar. A rotating core of fluid can appear inside the air-gap between the two boundary layers. The flow structure depends on Re_r and C_W, which are represented by the flow parameter κ. For a laminar flow, this parameter is defined as

$$\kappa_{lam} = C_W Re^{-0.5} \tag{5}$$

Soo [18] has shown that the tangential velocity of the rotating core of fluid is a function of $\tilde{r}$. If $\tilde{r} < \tilde{r}_0$, where $\tilde{r}_0 = \left(\frac{\kappa_{lam}}{\pi}\right)^{0.5}$, the rotating core of fluid does not appear in the air-gap, and the flow near the rotor is similar to the one obtained for a single rotating disk. Soo [18] has furthermore said that:

- If $\left(\frac{\kappa_{lam}}{\pi}\right)^{0.5} < 1$, the flow is a Batchelor-type flow.
- If $\left(\frac{\kappa_{lam}}{\pi}\right)^{0.5} > 1$, the flow is a Stewartson-type flow.

In a Batchelor-type flow [19], two boundary layers develop near each disk, separated by a rotating core of fluid. On the other hand, in a Stewartson-type flow [20], there is only a single boundary layer for the rotating disk, and the flow is very similar to the flow observed in the case of a disk rotating in still air.

2.2.4. Configuration IV

In this configuration, the spacing interval G is again wide, but the flow is turbulent. The structure of the turbulent flow is similar to the previous case. Some authors have defined the flow parameter as

$$\kappa_{tur} = C_W Re^{-0.8} \tag{6}$$

In order to characterize the flow, Owen [11], like Soo [18] for configuration II, has defined a parameter, such that $\tilde{r}_1 = \left(\frac{\kappa_{tur}}{0.219}\right)^{5/13}$. When $\tilde{r} < \tilde{r}_1$, the rotation of the fluid core becomes negligible, and the flow is a Stewartson-type flow [20].

3. Experimental study

3.1. Apparatus

In order to determine the heat fluxes on the rotating disk, we use infrared thermography and a thick wall method, which has been described in detail in [21]. In our experiments, the diameter of the rotating disk was

620 mm. Using a frequency regulator, its rotational velocity can range between 30 and 1000 rpm, which produced a rotational Reynolds number between 20,000 and 645,000. The thermocouples were connected to the rotating collector via a hollow 1 m shaft. Four infrared emitters with a short response time and a total power of 12 kW were placed on the bottom of the disk. As shown in Fig. 1, a polished box was placed to concentrate the maximum amount of radiative energy on the disk. In our experiments, a highly conductive material had to be used on the bottom of the rotating disk to homogeneize the heat power. We chose aluminum for its high thermal conductivity (200 $W\,m^{-1}\,K^{-1}$), but also for its density (2700 $kg\,m^{-3}$) and its mechanical properties, including an elastic modulus of 67,000 Pa. For the insulating material, we decided to use a layer of zircon, deposited on the aluminum via plasma projection. Plasma projection offers two essential features: a homogeneous depth and high temperatures to insure that the two materials adhere properly. In order to obtain the most homogeneous temperature at the zircon/aluminum interface and the highest radial gradient on the cooled surface, we estimated the thicknesses of the two materials: the aluminum was set at 43 mm and the zircon was set at 2.5 mm.

An aluminum disk measuring 620 mm in diameter was chosen for the stator. It was placed at distances ranging from 3 to 50 mm, far from the rotor. During testing, the stator was subjected to the radiative heat flux coming from the rotating disk. The stator was thus painted with a grey paint, whose emissivity was estimated to be $\epsilon_s = 0.65 \pm 0.03$.

Because of the method used, the rotor had to be visible through the stator. Therefore, an observation window in fluorspar is chosen for its high transmission coefficient of infrared waves. The fluorspar has a dimension of 290 × 20 mm. The rotor radii, which could be observed through this fluorspar window, ranged from 0.02 to 0.31 m. A hole ($D = 26$ mm) was pierced at the center of the stator to allow the passage of a pipe linked to a centrifugal blower. One diffuser and two pressure taps were placed between the blower and that pipe. The injected mass flow rate was regulated by creating a pressure loss at the blower suction chamber. Consequently, the imposed axial Reynolds numbers ranged from 8.3×10^3 to 41.6×10^3.

3.2. Procedure

3.2.1. Local Nusselt number calculation

To determine the local convective coefficients and the local Nusselt numbers, the parietal heat flux on the rotating surface can be obtained by solving the Laplace equation. Taking into account the axisymmetry of the problem, it can be written:

$$\frac{\partial^2 T(r,x)}{\partial r^2} + \frac{1}{r} \times \frac{\partial T(r,x)}{\partial r} + \frac{\partial^2 T(r,x)}{\partial x^2} = 0 \tag{7}$$

The zircon is meshed, and a difference-finite method is used. The boundary conditions applied are the surface temperatures recorded by the infrared camera and the interface temperatures recorded by the thermocouples. The axisymmetry of the problem allows us to impose the heat flux to zero on the boundary situated at $r = 0$ m. At $r = R_{ext}$, it is verified that the results are not influenced by the chosen boundary condition, due to a nearly monodimensional transfer. It is thus supposed that the temperature variation is linear from the aluminum/zircon interface to the cooled surface. In our tests, we observed 150 points with the

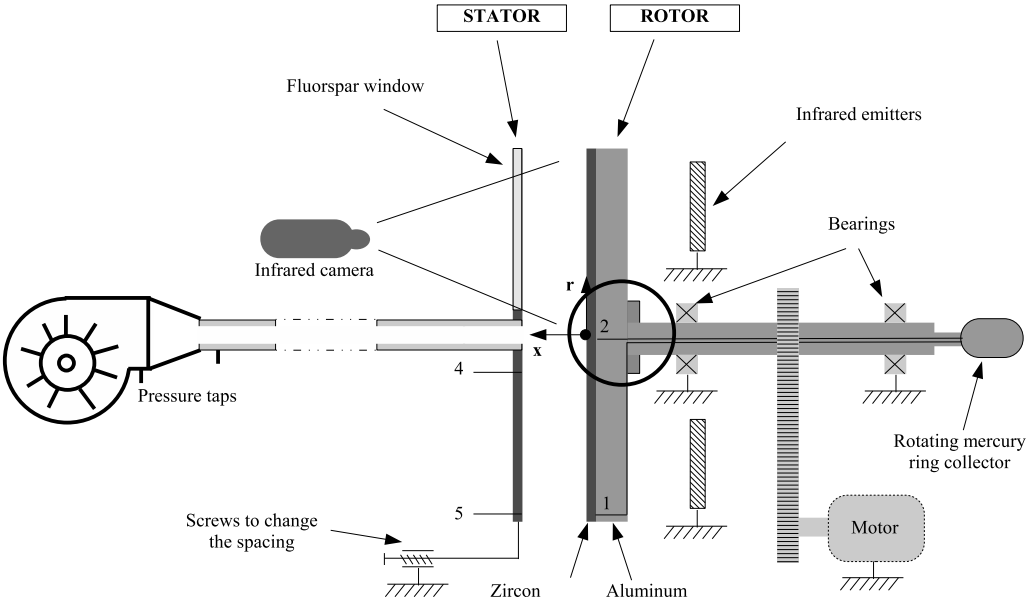

Fig. 1. Experimental set-up.

infrared camera. Because the results were independent of the mesh if the number of cells was equal to 30 or more, we chose a mesh with 30 cells in the x-direction.

The conductive heat flux is calculated based on the thermal gradient on the surface of the zircon, such that:

$$\varphi_{cd} = \lambda_{zir}\left(\frac{\partial T(r,x)}{\partial x}\right)_{x=0} \tag{8}$$

The radiative heat flux is considered to be the radiative heat flux exchanged between two parallel disks and is calculated using Ritoux's form factor F [22]:

$$\varphi_{rad} = \sigma\frac{F\varepsilon_r\varepsilon_s}{1-F^2(1-\varepsilon_r)(1-\varepsilon_s)}\left(T(r,x=0)^4 - T_{stator}^4\right) \tag{9}$$

where F is a function of the dimensionless spacing interval between disks, denoted G:

$$F = 1 + \frac{G^2}{2} - \sqrt{\frac{G^4}{4} + G^2 - 1} \tag{10}$$

The convective heat flux can be deduced by solving a thermal balance equation for each point on the disk surface, and the local Nusselt number is obtained:

$$Nu_r = \frac{\lambda_{zir}\left(\frac{\partial T(r,x)}{\partial x}\right)_{x=0} - \sigma\frac{F\varepsilon_r\varepsilon_s}{1-F^2(1-\varepsilon_r)(1-\varepsilon_s)}\left(T(r,x=0)^4 - T_{stator}^4\right)}{T(r,x=0)-T_\infty} \times \frac{r}{\lambda_{air}} \tag{11}$$

This formulation of the local Nusselt number is based on the ambient temperature. Owen and Rogers [11] observed that using this formulation is quite natural for discoidal systems with an inlet flow (imposed or not). However, they also proposed the use of the adiabatic surface temperature, defined as

$$T_{ad} = T_j + \frac{Pr^{1/3}\omega^2 r^2}{2C_p} \tag{12}$$

The temperature T_j is the temperature of the injected air, which in our tests was equal to the ambient temperature T_∞. The estimated maximum that can be attained with $[T_{ad} - T_\infty]_{max}$, for the maximal radius and velocity in our parameter range, is 0.5 K. The maximum relative difference between the local Nusselt numbers using T_∞ and T_{ad} can also be calculated, yielding:

$$0 < \frac{Nu_r(T_{ad}) - Nu_r(T_\infty)}{Nu_r(T_\infty)} < 2.5\% \tag{13}$$

As this result shows, the maximal difference is very low. Based on these observations, we chose the ambient temperature as the "reference" value for this study.

3.2.2. Global Nusselt number calculation

Several authors have defined the global Nusselt number as $\overline{Nu} = \frac{\bar{h}R}{\lambda_{air}}$. In our experiments, the mean heat transfer coefficient for the disk was calculated by integrating the local heat flux on the rotating surface. The following expression could be used to obtain the global Nusselt number:

$$\overline{Nu} = \frac{2}{R} \times \frac{\int_0^R Nu \times (T(r,x=0) - T_\infty)\mathrm{d}r}{\overline{T(r,x=0) - T_\infty}} \tag{14}$$

3.2.3. Temperature measurements on the rotor surface

Rotor temperatures were obtained using an AGEMA 900 infrared camera, situated one meter away from the disk. The camera observed the disk surface normally, with a measuring frequency of 35 Hz. To increase the importance of the infrared radiative flux emitted by the rotating disk, the disk surface was painted with a high emissivity black paint,whose emissivity was estimated such that $\varepsilon_r = 0.93 \pm 0.01$. During a test run, the infrared camera recorded the following flux I_r:

$$I_r = \tau_f\tau_a J_r + (1-\tau_a)I(T_\infty) + \tau_a\tau_f^2(1-\epsilon_r)I_{env} \tag{15}$$

The term J_r is the rotor radiosity, which includes all the signals emitted by the rotor and all reflections coming off it. The camera also recorded this rotor radiosity, altered by the air and fluorine transmission coefficients, plus an atmospheric term $I(T_\infty)$ and an environmental term I_{env}. The atmospheric term, $I(T_\infty)$, was estimated by measuring T_∞ using a thermocouple and the calibration law. The environmental term, I_{env}, was estimated by positioning a reflecting aluminum sheet in proximity to the surface. The rotor radiosity was estimated by solving a radiosity system equation, considering the air-gap as a closed system whose boundaries are the rotor, the stator and the fluorspar window, and the crown shaped by the air. All boundaries were considered to be grey surfaces. The rotor and the stator temperatures were measured with thermocouples and presumed uniform. The highest temperature on each surface was used in the calculations in order to maximize the calculated radiative heat flux. The temperature of the fluorspar window and the air in the air-gap were also presumed uniform and equal to the ambient temperature.

The temperature measurements with this method are not only dependent on the calibration law, the emissivity of the black paint, the air temperature and the air transmission coefficient, but also on the emissivity of the grey paint ε_s and the fluorspar transmission coefficient τ_f, set by the supplier at $\tau_f = 0.95 \pm 0.01$. In our temperature range, $323 < T < 353$ K, the absolute error is estimated to be 1 K.

3.2.4. Temperature measurements at the zircon/aluminium interface

As shown in Fig. 1, two thermocouples (denoted 1 and 2) – situated inside the two holes ($D = 3$ mm) at the bottom of the disk at the aluminium/zircon interface – were linked to an acquisition system by a four-channel rotating mercury ring collector. They were placed at two different radii: $r = 0$ and 0.3 m. The absolute error for the aluminium/zircon interface temperature is estimated at ± 0.3 K. As said

previously, the disk has been made with two different materials and their thicknesses have been calculated in order to get the most homogeneous temperature at the considered interface. Moreover, it has been checked that this temperature is constant and that a number of two thermocouples is enough to allow a reliable calculation, namely during the validation tests presented in the Section 3.2.8.

3.2.5. Ambiant temperature measurement

The reference air temperature T_∞ was measured by a type K thermocouple placed outside the test-rig, far enough from the rotating system. The absolute error for the air temperature is estimated at ±0.3 K and was directly connected to the acquisition system.

3.2.6. Temperature measurement in the stator

Two T-type thermocouples were directly linked to the acquisition system (numbers 3 and 4 in Fig. 1). They were placed at radii of 0.05 and 0.3 cm. The absolute error for the stator temperature is estimated at ±0.3 K.

3.2.7. Flow rate measurement

To determine how the impinging jet modifies the local and mean heat transfers, the flow rate was estimated by measuring the pressure drop through the diffuser with a micro-manometer according to $\Delta H_{\mathrm{mmH_2O}}$. At the same time, velocities were measured at the different radius of the outlet section using a Pitot tube, which gives the pressure drop according to $\Delta H_{\mathrm{pitot}}$:

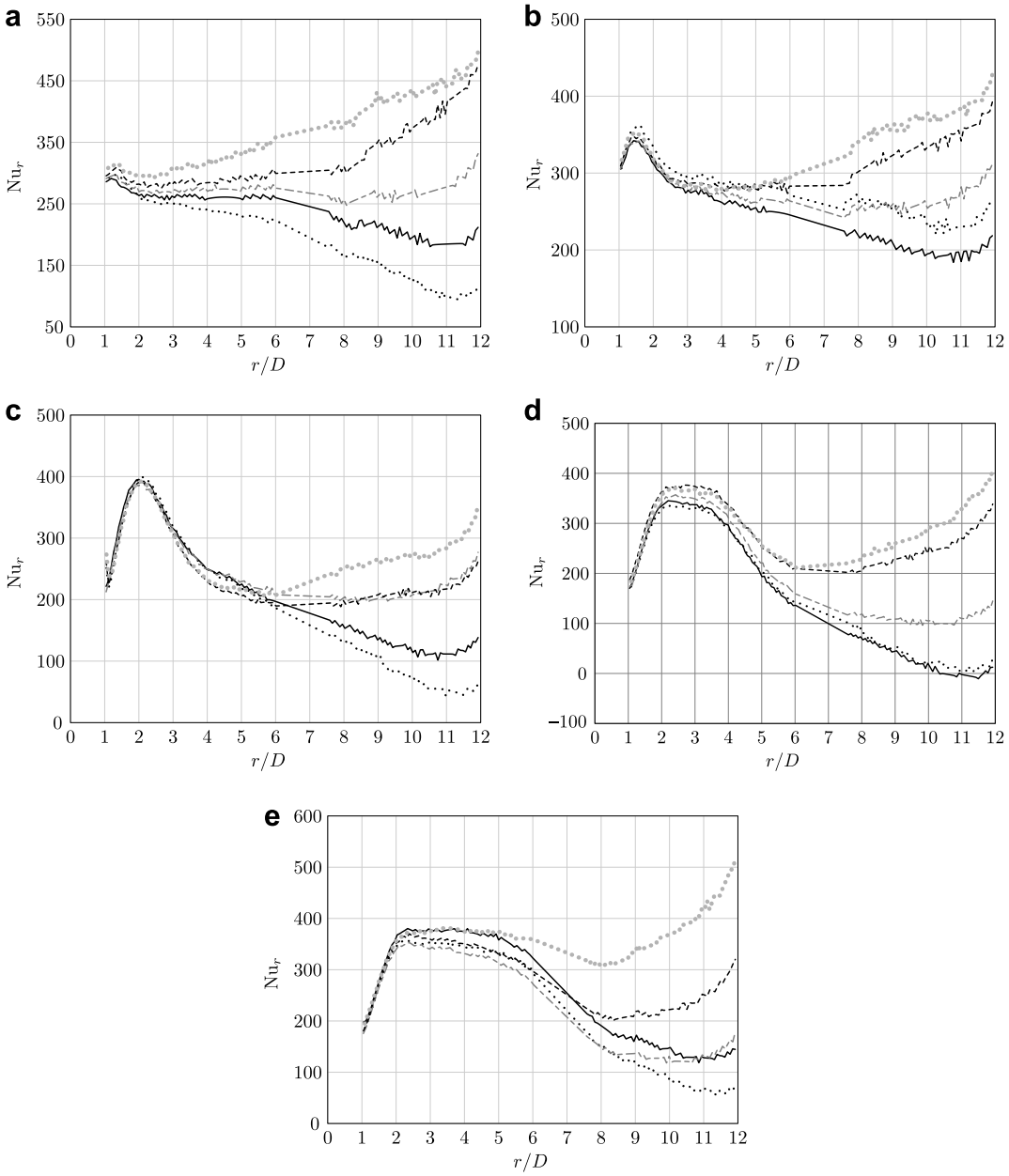

Fig. 2. Experimental results concerning the local Nusselt numbers with $Re_j = 41.6 \times 10^3$ and $G = 0.01$ (a), $G = 0.02$ (b), $G = 0.04$ (c), $G = 0.08$ (d), $G = 0.16$ (e). (. . . . . .) $Re = 0.2 \times 10^5$; (——) $Re = 1.29 \times 10^5$; (— —) $Re = 2.58 \times 10^5$; --- $Re = 3.87 \times 10^5$; (●) $Re = 5.16 \times 10^5$.

$$V(r) = \sqrt{\frac{2\rho_{H_2O} g \Delta H_{pitot}}{\rho_{air}}} \quad (16)$$

By integrating these velocity profiles, the mass flow rate and the mean velocity V_j in the pipe can be deduced:

$$V_j\ (\mathrm{m\ s^{-1}}) = 2.881 \times \sqrt{\Delta H_{mmH_2O}} \quad (17)$$

During experimentation, the desired pressure drop could be selected by adjusting the valve near the blower.

3.2.8. Error analysis and validation

By taking into account all the uncertainties mentioned above, the mean relative uncertainty for the local Nusselt number is estimated to 12%. The same uncertainty can also be calculated for the global Nusselt numbers. For the rotational velocity, the absolute error according to the supplier is 2 rpm in the range 0–1000 rpm, which means a maximal value of 7% for the relative uncertainty of *Re*. The method used to link the mean velocity in the jet to the pressure drop through the diffuser yields a maximal relative error of 10% for the jet Reynolds number. To insure that the experimental set-up would produce reliable results, a preliminary study was conducted on a single rotating disk configuration. This is a well-known problem and results compare favorably to those of Dorfman [5] and Cardone [6] for laminar and turbulent flows.

4. Results

This section reports the results for the convective heat transfer on the rotor. The jet diameter was set at $d = 26$ mm. The jet Reynolds number Re_j formulae was set to 41.6×10^3, the rotational Reynolds number *Re* ranged from $Re = 0.2 \times 10^5$ to 5.16×10^5. The dimensionless spacing interval G varied between 0.01 and 0.16.

4.1. Local Nusselt numbers

Fig. 2a–e show the local Nusselt numbers Nu_r versus the dimensionless position r/D. Each of the charts represents one dimensionless spacing interval G, and each curve represents a fixed rotational Reynolds number *Re*. A peak in the local Nusselt numbers can be seen at the lowest dimensionless radii. Indeed, for $G = 0.01$ on Fig. 2a and for $r/D = 1.3$, the local Nusselt numbers reach a local maxima, whatever the rotational speed. The same observation can be made for $G = 0.02$ and 0.04 (Fig. 2b and c). For the two greatest spacing intervals $G = 0.08$ and 0.16 (Fig. 2d and e), the value no longer peaks, but instead increases, then remains quite constant, before diminishing. In addition, the radial position, where the local maximum is situated, depends on G. In fact, for $G = 0.02$, the local maximum is reached when r/D is about 1.5 and for $G = 0.04$ when r/D is about 2. For $G = 0.08$ and 0.16, Nu_r also increases with r/D until $r/D = 2$. When the r/D is high enough, the curves separate, demonstrating that Nu_r is a function of *Re*. In addition, when the space between the curves widens, the local convective heat transfer is an increasing function of *Re*, whatever G. With low *Re* values, Nu_r decreases with r/D, whereas it increases with higher *Re* values. Furthermore, for a fixed G, varying the rotational Reynolds number does not cause any change in Nu_r at low radii. When G is constant, the results are independent of *Re* in the central area of the disk. This phenomenon is more obvious when G is low than when it is high. However, when comparing the local Nusselt numbers attained in the zone independent of *Re*, it is obvious that this local maxima depends on G.

As shown in Fig. 3, when *Re* is set to 3.87×10^5, the results can be divided into two groups. For $G = 0.01$ and 0.02, the local Nusselt numbers for most of the disk surface remain quite constant at about $Nu_r = 300$. At higher radii, Nu_r increase with r/D. Moreover, for these two values of G, the local Nusselt numbers are nearly identical for the entire disk surface. However, for the three highest G values, the evolution of the Nu_r values is more pronounced, with a significant increase at lower radii. The three profiles come together again at high radii, but the values are lower than for $G = 0.01$ or 0.02. So, depending on G, Nu_r evolve differently. The chart in Fig. 3 also demonstrates that the size of the area that is clearly influenced by the impinging jet is an increasing function with G. The local maxima reached with narrow spacing intervals are lower than those reached for wider intervals, although at the outer radii the values can be higher for narrow intervals.

For the five tested dimensionless spacings, the experimental temperature profiles are given on Fig. 4. The dotted lines show the aluminum/zircon interface temperatures which are measured by the thermocouples. Values are interpolated and it can be seen that the temperature is constant at this location. The surface temperatures, determined

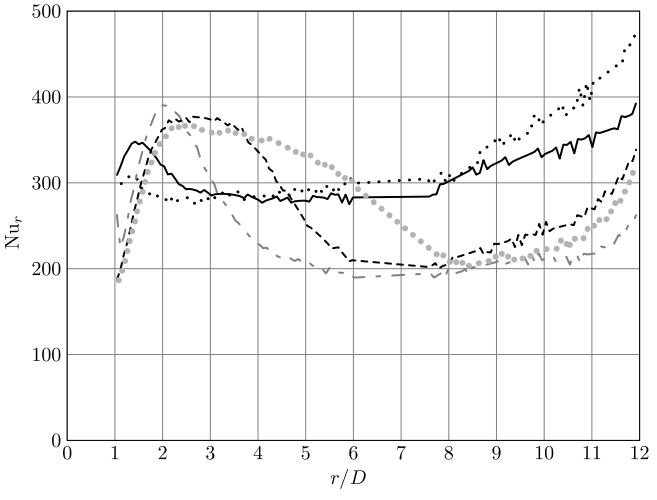

Fig. 3. Experimental results concerning the local Nusselt numbers; $Re_j = 41.6 \times 10^3$; $Re = 3.87 \times 10^5$. (.....) $G = 0.01$; (——) $G = 0.02$; (—·—) $G = 0.04$; (---) $G = 0.08$; (●) $G = 0.16$.

with the infrared camera, are also plotted. Those results show that the apparatus allow to directly have an idea of the heat transfer coefficient by observing the surface temperatures. In fact, their evolution are the opposite of the heat transfer coefficient evolution.

4.2. Global Nusselt numbers

The evolution of the global Nusselt numbers was studied by varying the two parameters: Re and G. The experimental results are presented in Fig. 5, where $\overline{Nu}$ is plotted versus the dimensionless spacing interval G for each rotational velocity studied.

4.2.1. Influence of the dimensionless spacing

As shown in Fig. 5, for $Re = 0.2 \times 10^5$, $\overline{Nu}$ increases between $G = 0.01$ and 0.02, while for the other rotational velocities $\overline{Nu}$ decrease with G. As G increases, the global Nusselt number decreases, until G reaches between 0.04 and 0.08, whatever the value of Re. At this point, $\overline{Nu}$ begins to increase with G. For the local Nusselt numbers shown in Fig. 3, the results could be divided into two groups, whose transition boundary was associated to a critical G, corresponding to the minima of the global Nusselt numbers. For small dimensionless spacing intervals, an increase in G clearly causes an increase in the local maxima attained at the low radii, but also leads to a very significant decrease in the convective heat transfer at outer radii, which in turn causes the global Nusselt numbers to decrease too. On the other hand, at higher G values, an increase in G leads to an increase in the size of the jet-dominated area, near the stagnation point. The local Nusselt numbers are thus enhanced in this area, resulting in an increase in the global Nusselt number.

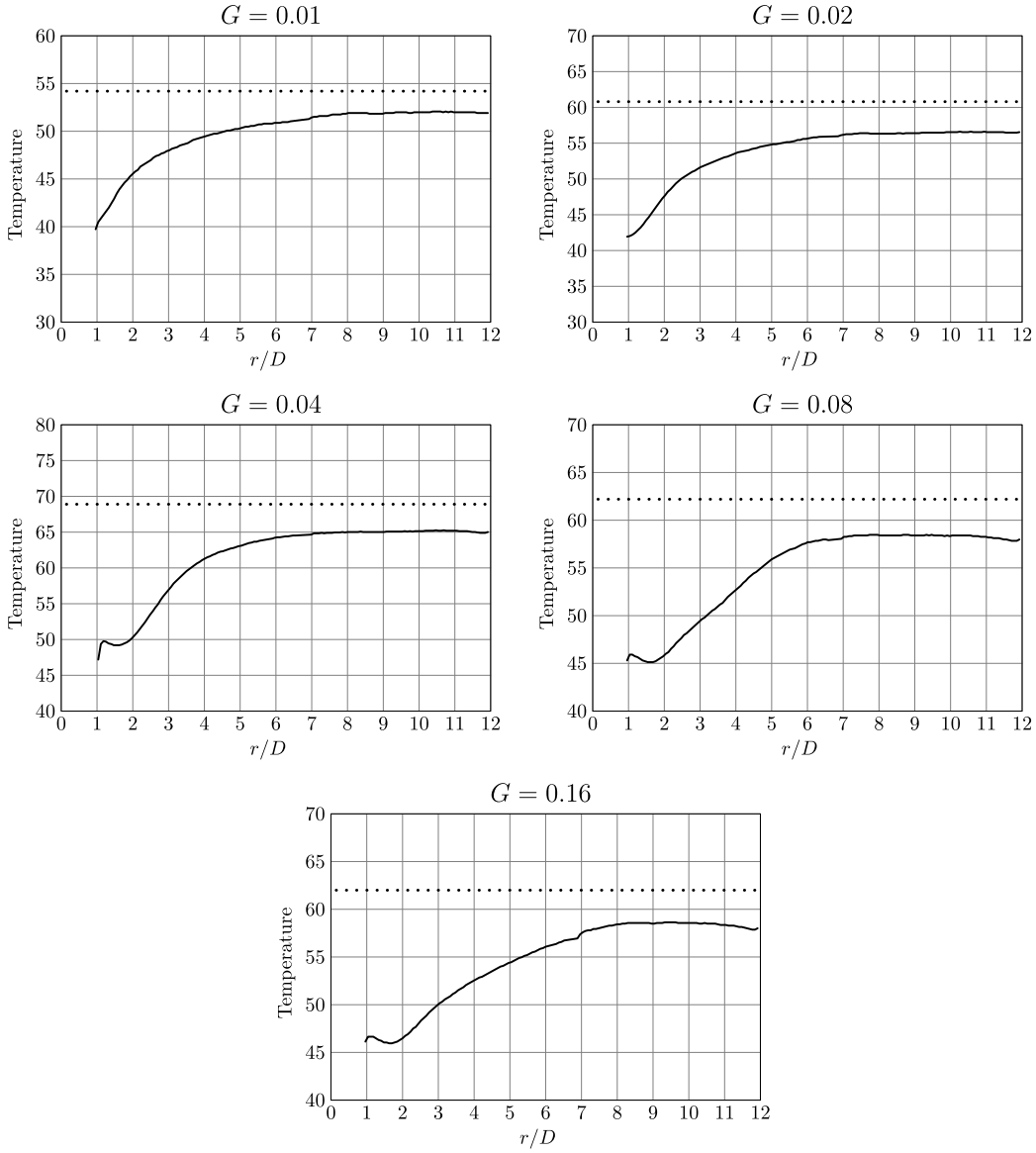

Fig. 4. Temperature (°C) profiles measured on the rotor for $Re = 3.87 \times 10^5$ and $Re_j = 41.7 \times 10^3$; (——) surface temperatures; (. . . . . .) aluminum/zircon interface temperatures.

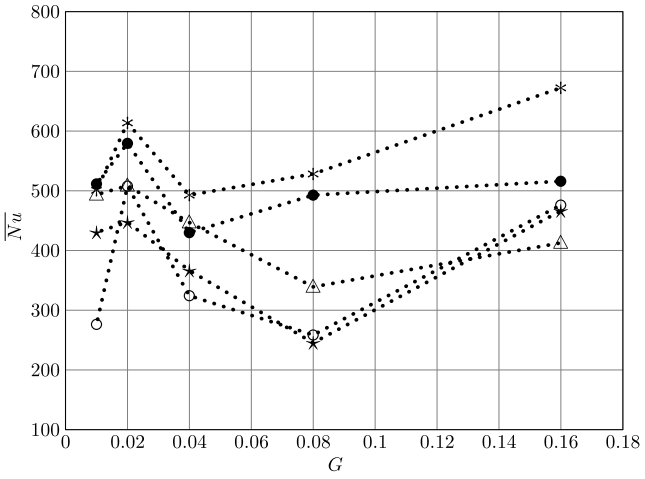

Fig. 5. Experimental results concerning the global Nusselt numbers for $G = 0.01$. (○) $Re = 0.19 \times 10^5$; (★) $Re = 1.29 \times 10^5$; (△) $Re = 2.58 \times 10^5$; (●) $Re = 3.87 \times 10^5$; (*) $Re = 5.16 \times 10^5$.

4.2.2. Influence of the rotational velocity

As shown in Fig. 5, the global Nusselt number for the entire disk surface seems to be an increasing function of Re, whatever the dimensionless spacing interval, although inversions are sometimes produced on Nu_r at the outer radii by increasing the rotational velocity values.

4.3. Interpretation

Owen [11] has summarized the results of several authors concerning the flow structure in a discoidal system's air-gap. His summary highlights the fact that three parameters are needed to characterize the flow: $\phi(\tilde{r})$ for small dimensionless spacing intervals G, and $\tilde{r}_0$ and $\tilde{r}_1$ for large intervals. The problem is determining the boundary between the small and large G values. Several authors have described a transition for a dimensionless spacing interval of about $G = 0.02$. The three parameters mentioned above can be expressed as follows:

$$\phi(\tilde{r}) = \frac{GC_W}{2\pi \times (Re_G \tilde{r})^2} \tag{18}$$

$$\tilde{r}_0 = \left(\frac{\kappa_{lam}}{\pi}\right)^{0.5} \tag{19}$$

$$\tilde{r}_1 = \left(\frac{\kappa_{tur}}{0.219}\right)^{5/13} \tag{20}$$

In order to emphasize the following discussion, Fig. 6a and b show how the flow develops inside the air-gap for two cases. On the one hand, Fig. 6a gives an idea of the flow in the air-gap when the spacing and the rotation are relatively low compared to the jet mass flow rate. The flow is thus totally centrifugal in the air-gap. On the other hand, Fig. 6b shows the flow when the rotation has a more pronounced effect than the jet in the air-gap. This can be the case when the spacing and the rotational speed are high. The flow is firstly centrifugal in the whole thickness of the air-gap until a critical radius. Then an inlet centripetal flow develops near the stator. Also, the rotational effects are more pronounced near the rotor. The two previous flows are delimited with one of the criteria (18)–(20) in order to calculate the critical radii, depending on the kind of flow which is encountered in the air-gap. For a relatively narrow spacing interval, the Soo criterion (18) [18] is used to know when the flow changes from centrifugal to centripetal near the stator. And for a relatively wide interval, the parameters (19) and (20) are used when the flow is respectively laminar or turbulent.

4.3.1. Narrow dimensionless spacing intervals

In our parameter range, $\phi(\tilde{r})$ was calculated for narrow dimensionless spacing intervals, such as $0.01 < G < 0.02$. The minimum value for $\phi(\tilde{r})$ was thus estimated to be 0.3 for the chosen axial Reynolds number. However, according to Soo [18], an inlet flow from the outside of the air-gap only occurs when $\phi < 0.1$. So, in this configuration, the flow appears to be centrifugal throughout the air-gap for $G = 0.01$ and 0.02. The rotational velocity is not high enough to permit an inlet flow at the outer radii for that injected mass flow rate. Clearly, the local Nusselt number profiles do not vary as much as for higher G values, and there are no significant changes in the curve slope, except in the central area, where the changes are due to the presence of the jet.

4.3.2. Wide dimensionless spacing intervals

For wide dimensionless spacing intervals, the following equations $\tilde{r} = \tilde{r}_0$ and $\tilde{r} = \tilde{r}_1$ were solved for each configuration. In our range of parameters, the first equation does not lead to any real physical solution because the calculated critical radii fall outside of the disk surface. However, the

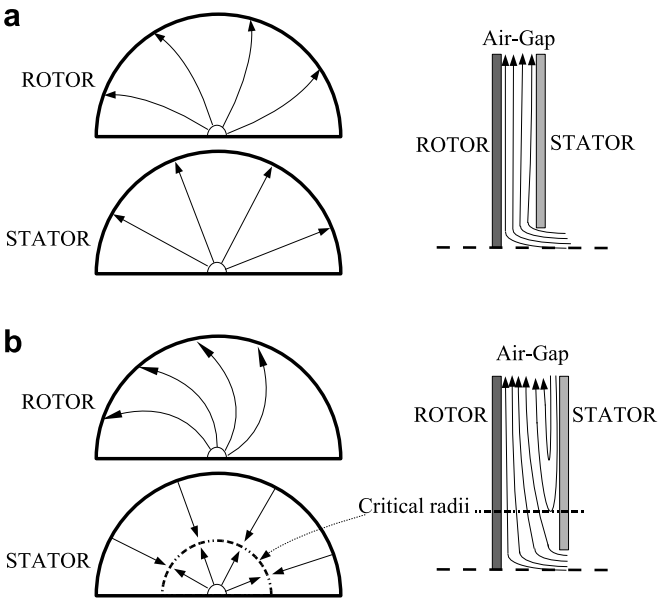

Fig. 6. Illustrations of the flow structure inside the air-gap for a narrow intervals (a) and wide intervals (b).

second equation does provide a set of critical values which are shown in Table 1.

The lowest Re_j at the center of the stator is $8{,}3 \times 10^4$ and corresponds to a turbulent flow inside the supply pipe. Consequently, the flow inside the rotor's boundary layer is turbulent, whatever the value of G. For a turbulent flow, the radii $(r/D)_1$ correspond to noticeable changes in our experimental results. As shown in Fig. 7, these radii can be used to divide our profiles into two groups. As shown in our profiles, the limit between the zones is situated just after the significant increase in Nu_r due to the added jet in the central area and just before the increase due to the rotation at outer radii. According to Owen's definition of $(r/D)_1$ [11], the flow is at first totally centrifugal in the central area of the disk; only when $(r/D) > (r/D)_1$ does a rotating core of fluid and an inlet flow appear near the stator.

Since our results for convective heat transfers on a rotating disk are strongly connected to the flow pattern, it is interesting to look at how these two elements are correlated.

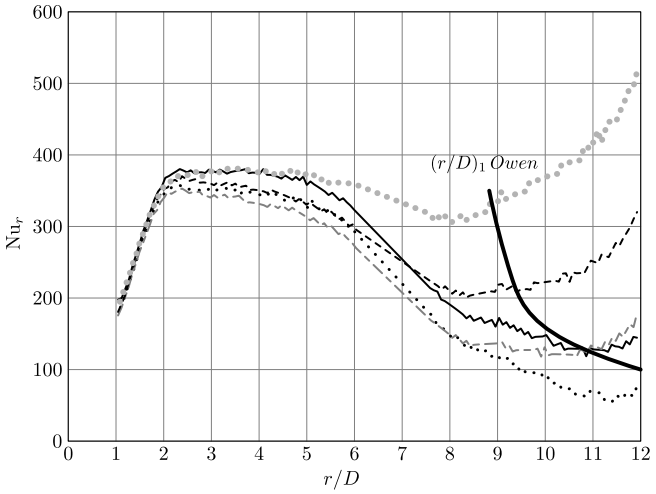

Fig. 7. Comparison between local Nusselt numbers and bibliography data about the flow [11]; $Re_j = 41.6 \times 10^3$ and $G = 0.16$; (.....) $Re = 0.2 \times 10^5$; (——) $Re = 1.29 \times 10^5$; (—–) $Re = 2.58 \times 10^5$; (---) $Re = 3.87 \times 10^5$; (●) $Re = 5.16 \times 10^5$.

4.3.3. Correlation between heat transfer and flow

Compared to the no-jet configuration [21] where there is no real flow near the stagnation point, a mass flow rate imposed in the air-gap leads to a totally centrifugal flow at this location and to a significant increase in the convective heat transfer, whatever the G or Re values. Some authors [9] have demonstrated that the vortices generated at the pipe outlet break up the boundary layer near the rotor and accelerate the air renewal, thus enhancing the heat transfer. Modifying the rotational velocity has no influence on convective heat transfer because tangential velocity is very low near the center. The size of that jet-dominated area near the stagnation point also strongly depends on G, essentially because the width of the air jet is more significant as the spacing between the pipe outlet and the rotor gets larger.

In all cases, as r increases, the air gradually begins to rotate, which helps to explain why Re has an influence on Nu_r at higher radii. But in our case, the evolution of the flow structure and the heat transfer is not the same whatever G. For $G = 0.01$ and 0.02, the flow is totally centrifugal throughout the air-gap. Soo's observations [18] are confirmed by our results. For wider intervals, the centrifugal flow imposed by the jet is confined near the rotor, with an inlet flow occurring near the stator. The rotation of the rotor causes a rotating core of fluid to appear in the air-gap when the rotational speed is high enough. This flow is a Batchelor-type flow [19], as has been observed in the air-gap without any jet impingement. In this area, the parietal stress decreases, which explains why the local Nusselt numbers at high radii are lower in wide spacing configurations (Fig. 3). When G increases once again, the convective heat transfer also increases, and the flow becomes a Stewartson-type flow [20]. In this flow, the boundary layers are disjointed, and the rotating core of fluid progressively disappears.

The global Nusselt number increases with Re, whatever the value of G, essentially due to the local increases observed at outer radii. The global Nusselt numbers first decrease as G increases, until Nu_r value reaches its minimum value. This decrease is caused by the appearance of a rotating core of fluid at outer radii, thus diminishing the local heat transfer. Of course, increasing G values lead to a larger jet-dominated area. However, when calculating the global Nusselt number, the higher the radius, the greater the effect of a Nu_r modification. Clearly, events near the center do not have a very significant effect on the global Nusselt number.

Table 1
Critical radii $(r/D)_1$ for the flow change in the turbulent case [11]

Re_j ($\times 10^{-3}$)	Re ($\times 10^{-5}$)				
	0.2	1.29	2.58	3.87	5.16
41.6			10.4	9.2	8.8

5. Conclusion

This research was part of a general study about the convective heat transfers on a rotor surface in different configurations of a discoidal system. We chose to vary the spacing interval and the rotational velocity in order to examine the influence of a jet on the local and global convective heat transfers on a rotor in such a system. Our heat transfer measurements confirm the data about flow structure found in the bibliography. The local convective heat transfer was enhanced near the stagnation point at low rotational velocities, where the influence of the jet is preponderant. At high radii, the local Nusselt numbers were shown to depend on both jet and rotation. The influence of the spacing interval on global Nusselt numbers was also

highlighted by our results, with these numbers reaching a minimum value depending on the rotational velocity and on the spacing interval. In our parameter range, adding a jet is always advantageous for the heat transfer, as confirmed by the global Nusselt numbers. Our results underline the importance of the influence of the rotational speed and the dimensionless spacing interval between the two disks for a fixed injected mass flow rate. The addition of a jet impinging the center of the rotor is advantageous for the heat transfers, primarily near the stagnation point. In order to complete this research and to improve the cooling at outer radii, a study will determine velocities in the air-gap with the use of PIV and another work with several impinging jets added at positive radii could be done.

References

[1] T. Von Karman, Über laminar und turbulente reibung, Math. Mech. 1 (1921) 244–252.

[2] S. Goldstein, Dans Camb. Philos. Soc. 31 (1935) 232.

[3] E.C. Cobb, O.A. Saunders, Heat transfer from a rotating disk, Dans Proc. R. Soc. A 236 (1956) 343–351.

[4] P.D. Richardson, O.A. Saunders, Studies of flow and heat transfer associated with a rotating disk, J. Mech. Eng. SC. 5 4 (1963) 336–342.

[5] L.A. Dorfman, Hydrodynamic Resistance and Heat Loss from Rotating Solids, Edinburgh/London, 1963.

[6] G. Cardone, T. Astarita, G.M. Carlomagno, Infrared heat transfer measurements on a rotating disk, Opt. Diagn. Eng. 1 (1996) 1–7.

[7] L. Huang, M.S. El-Genk, Heat transfer and flow visualization experiments of swirling, multi-channel, and conventional impinging jets, Int. J. Heat Mass Transfer 41 (1998) 583–600.

[8] M. Fenot, J.J. Vullierme, E. Dorignac, Local heat transfer due to several configurations of circular air jets impinging on a flat plate with and without semi-confinement, Int. J. Thermal Sci. 44 (2005) 665–675.

[9] M. Angioletti, R.M. Di Tommaso, E. Nino, G. Ruocco, Simultaneous visualization of flow field and evaluation of local heat transfer by transitional impinging jets, Heat Mass Transfer 46 (2003) 1703–1713.

[10] Y.M. Chen, W.T. Lee, S.J. Wu, Heat (mass) transfer between an impinging jet and a rotating disk, Heat Mass Transfer 34 (1998) 195–201.

[11] J.M. Owen, M.H. Rogers, Flow and heat transfer in rotating disk systems, Rotor–Stator Systems, vol. 1, 1989.

[12] C.O. Popiel, L. Boguslawski, Local heat transfer from a rotating disk in an impinging round jet, J. Heat Transfer 108 (1986) 357–364.

[13] B.P. Axcell, C. Thianpong, Convection to rotating disks with rough surfaces in the presence of an axial flow, Exp. Therm. Fluid Sci. 25 (2001) 3–11.

[14] H. Iacovides, J.W. Chew, Heat transfer and flow visualization experiments of swirling, multi-channel, and conventional impinging jets, Int. J. Heat Fluid Flow 14 (2) (1993) 146–154.

[15] M. Djaoui, R. Debuchy, A. Dyment, Heat transfer in a rotor–stator system with a radial inflow, Eur. J. Mech. B: Fluid 20 (2001) 371–398.

[16] S. Poncet, R. Shiestel, Numerical modeling of heat transfer and fluid flow in rotor–stator cavities with throughflow, Int. J. Heat Mass Transfer 50 (2007) 1528–1544.

[17] E.M. Sparrow, J.L. Goldstein, Effect of rotation and coolant throughflow on the heat transfer and temperature field in an enclosure, J. Heat Transfer 98 (1976) 387–394.

[18] S.L. Soo, Laminar flow over an enclosed rotating disk, Trans. ASME 80 (1959) 287–296.

[19] G.K. Batchelor, Note on a class of solutions of the Navier–Stokes equations representing steady rotationally-symmetric flow, Quart. J. Mech.: Appl. Math. 5 (1951) 29–41.

[20] K. Stewartson, On the flow between two rotating coaxial disks, Dans Camb. Philos. Soc. 49 (1953) 333–341.

[21] J. Pellé, S. Harmand, Heat transfer measurements in an opened rotor–stator system air-gap, Exp. Therm. Fluid Sci. 31 (2006) 165–180.

[22] G. Ritoux, Evaluation numérique des facteurs de forme, Rev. Phys. Appl. 17 (1982) 503–515.